Computational and Structural Biotechnology Journal 23 (2024) 1311–1319

Contents lists available at ScienceDirect

Computational and Structural Biotechnology Journal

journal homepage: www.elsevier.com/locate/csbj

Research Article

Exploring key features of selectivity in somatostatin receptors through molecular dynamics simulations

C. Guccione, S. Gervasoni *, I. Öztürk, A. Bosin, P. Ruggerone, G. Malloci *

Department of Physics, University of Cagliari, Monserrato (Cagliari), 09042, Italy

ARTICLE INFO

Keywords:
Somatostatin receptors
Precision medicine
Theranostics
Molecular dynamics simulations
Structure-based drug discovery

ABSTRACT

Somatostatin receptors (SSTRs) are widely distributed throughout the human body and play crucial roles in various physiological processes. They are recognized as key targets for both radiotherapy and radiodiagnosis due to their overexpression in several cancer types. However, the discovery and design of selective drugs for each of the five isoforms have been significantly hindered by the lack of complete structural information. In this study, we conducted a systematic computational analysis of all five SSTRs in complex with the endogenous ligand somatostatin to elucidate their structural and dynamic features. We thoroughly characterized each isoform using available experimental structures for SSTR2 and SSTR4, as well as AlphaFold2 models for SSTR1, SSTR3, and SSTR5. By performing multi-copy μs-long molecular dynamics simulations, we examined the differences and similarities in dynamical behavior and somatostatin binding among all SSTRs. Our analysis focused on understanding the opening and closing movements of the extracellular loop 2, which are crucial for ligand binding and recognition. Interestingly, we observed a unique conformation of somatostatin within the binding pocket of SSTR5 in which the loop can partially close, as compared to the other isoforms. Fingerprint analyses provided distinct interaction patterns of somatostatin with all receptors, thus enabling precise guidelines for the discovery and development of more selective somatostatin-based pharmaceuticals tailored for precision medicine therapies.

1. Introduction

Precision medicine aims to tailor therapeutical approaches to match "the right drug for the right patient at the right time" [1]. This approach considers individual genetic, phenotypic, and psychosocial characteristics [2–5], offering several advantages such as considerable off-target effects reduction [6]. However, the effectiveness of precision medicine depends significantly on the availability of drugs tailored to their targets [7,8].

One effective strategy involves targeting different isoforms of proteins that serve as good biomarkers for certain diseases [9]. Somatostatin receptors (SSTRs) are a prime example in this context. Belonging to the class A G-protein-coupled receptors (GPCRs), SSTRs exist in five isoforms: SSTR1, SSTR2, SSTR3, SSTR4, and SSTR5, sharing common structural features with sequence identities ranging approximately in the range 40–60% (see Table 1) [10]. Phylogenetic analysis groups SSTRs into two sub-families: SRIF1 (SSTR2, 3, 5) and SRIF2 (SSTR1, 4) [10]. The endogenous agonist for SSTRs is somatostatin [11], a cyclic peptide hormone that exists in 14-residues (SST14) or 28-residues active forms (Fig. S1A) [10].

SSTRs are widely expressed throughout the human body (Fig. 1), regulating a variety of physiological functions [10]. However, they are also known to be generally involved in the progression of neuroendocrine tumors [13]. For this reason, several compounds have been developed to specifically target each isoform. More specifically:

- SSTR1 primarily affects prolactin and calcitonin secretion [14] and is predominantly expressed in prostate cancer [15]. While some somatostatin analogs are known to preferably bind this receptor [16], such as pasireotide (Fig. S1D) [17], at present there are no pharmaceuticals approved specifically for SSTR1.
- SSTR2 is the most prevalent isoform, regulating processes like growth hormone, insulin, glucagon, and stomach acid secretion [18]. It is overexpressed in various cancers, especially gastroenteropancreatic neuroendocrine tumors [19]. As to date, a few pharmaceutical compounds targeting SSTR2 have been approved (see below).

* Corresponding authors.
E-mail addresses: silvia.gervasoni@dsf.unica.it (S. Gervasoni), giuliano.malloci@dsf.unica.it (G. Malloci).

https://doi.org/10.1016/j.csbj.2024.03.005
Received 31 January 2024; Received in revised form 7 March 2024; Accepted 7 March 2024
Available online 18 March 2024
2001-0370/© 2024 The Authors. Published by Elsevier B.V. on behalf of Research Network of Computational and Structural Biotechnology. This is an open access article under the CC BY-NC-ND license (http://creativecommons.org/licenses/by-nc-nd/4.0/).

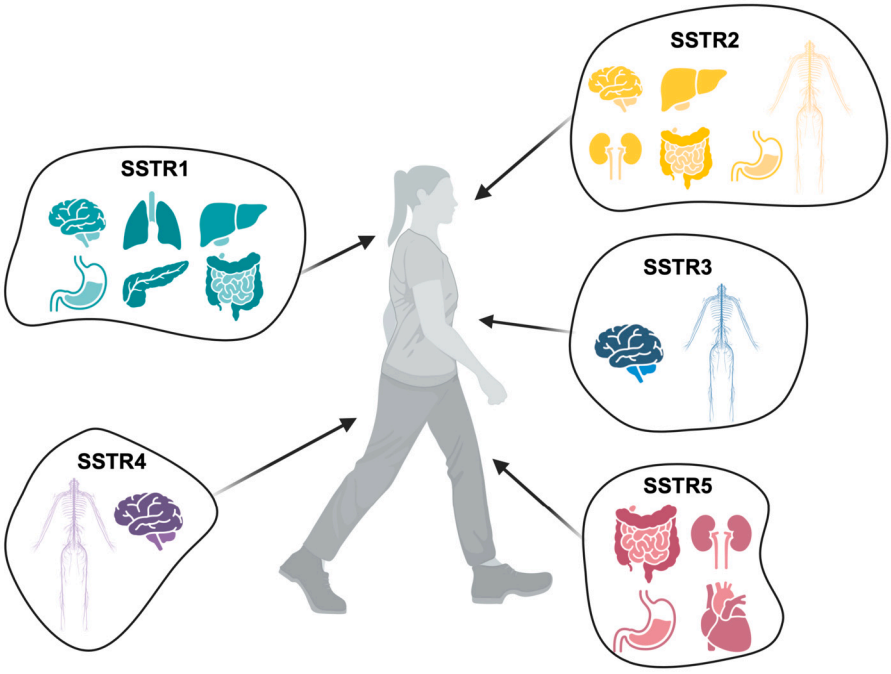

Fig. 1. Bio-distribution of the five SSTR isoforms in the human body (image generated with BioRender).

Table 1
Sequence identity matrix (percentages computed with ClustalOmega [12]).

	SSTR2	SSTR3	SSTR4	SSTR5
SSTR1	60	46	45	48
SSTR2	–	44	45	51
SSTR3	–	–	49	52
SSTR4	–	–	–	56

- SSTR3 inhibits cell proliferation and induces apoptosis [14], serving as a biomarker for non-functioning pituitary adenomas [20]. While there are no approved drugs specific for this isoform, a promising cyclic hexapeptide pan-SSTR agonist with high affinity for SSTR3 has been recently identified (ITF2984) [20].
- SSTR4 is the least expressed in cancer [21], but uniquely mediates analgesic and anti-inflammatory effects of somatostatin [22]. SSTR4 agonists like J-2156 (not yet approved) offer a potential alternative to opioids for chronic pain reduction, being expressed in the central and peripheral nervous system [23].
- SSTR5, similar to SSTR2, is mainly found in the brain, pituitary glands, pancreas, and gastrointestinal tract [14]. It is often co-expressed with SSTR2 in neuroendocrine breast cancer [24]. A potential antagonist for the control of glycemia, named S5A1, shows a subnormal affinity for SSTR5 [25].

Approved FDA drugs targeting SSTRs are either peptides (*e.g.*, octreotide [26], lanreotide [27], pasireotide [28]), or non-peptides (*e.g.*, paltusotine [29], see Fig. S1B-E), sharing a β-sheet portion featuring an aromatic group (typically tryptophan) and a basic positively charged moiety (for example, a lysine) accommodated in the deepest part of the binding pocket (Fig. 2A) [30]. These structural features are exploited in developing radiopharmaceutical drugs for cancer therapy and diagnosis [18,31].

Knowledge of the 3D structure of SSTRs is crucial in the development of compounds targeting specifically each isoform. Computational approaches combining homology modeling and molecular docking have provided insights into ligand binding to different SSTR isoforms [33–37]. Recent experimental structures of SSTR2 and SSTR4

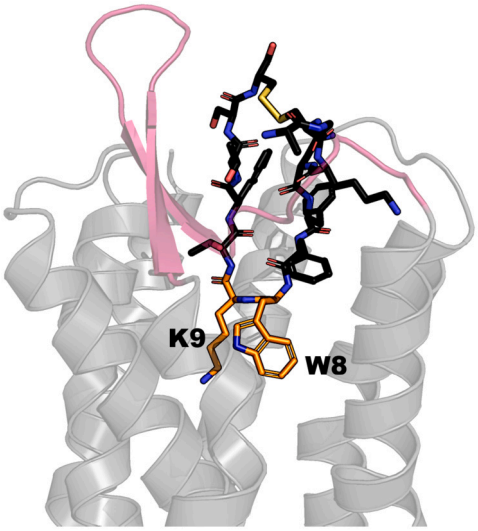

Fig. 2. Somatostatin (black sticks) bound to the binding pocket of SSTR2 (gray cartoon). The aromatic group (tryptophan) and the positively charged moiety (lysine) are highlighted in orange. The ECL2 is highlighted in warmpink. Experimental structure taken from PDB ID 7T10 [32].

[32,38] (see Table S1 for the complete list of available structures) have shed light on key structural features of somatostatin binding and its agonists or antagonists. The extracellular loop 2 (ECL2) was found to play a significant role in ligand binding and stabilization. In the case of SST14 and peptide analogues, the difference in the orientation of the disulfide bridge was reported to be peculiar for each receptor-ligand complex [30]. Molecular insights into the coupling with the G-protein, ligand selectivity and receptor activation were additionally provided [32].

Despite these precious insights, a comprehensive structural and dynamic characterization of all five isoforms is lacking. Leveraging available structural data, we previously conducted molecular dynamics (MD) simulations of SSTR2 with somatostatin analogs [39] and radiopharmaceutical compounds [31]. In this study, we systematically investigated the dynamics of all SSTR isoforms interacting with the endogenous ag-

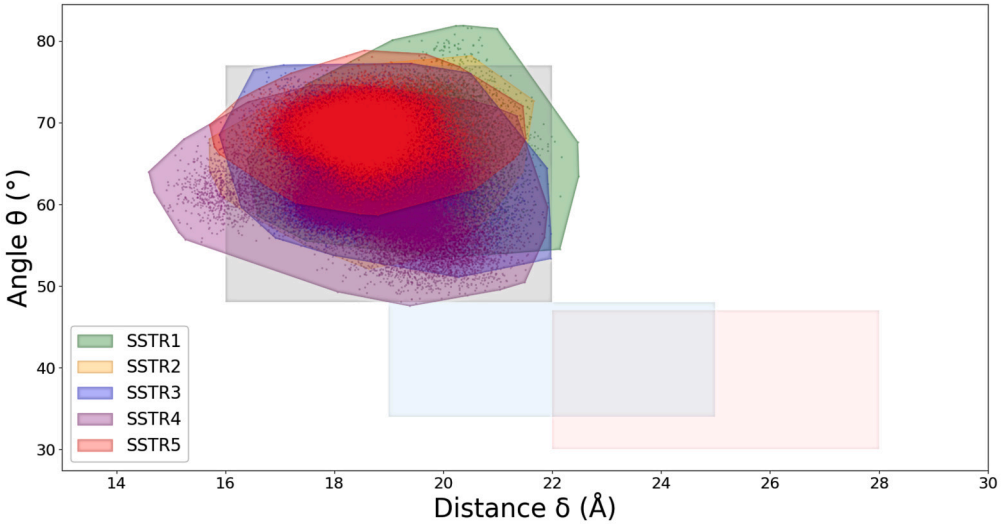

Fig. 3. Scatter plot of the active region for SSTRs. The gray area represents the active (agonist-bound) region (16–22 Å, 48–77°), the blue area is the inactive (antagonist-bound) region (19–25 Å, 34–48°) and the red area is the *apo* region (22–28 Å, 30–47°) [43].

onist SST14. Using experimental co-structures of SSTR2 and SSTR4 and AlphaFold2 [40] models for the others, we characterized receptor structures and their binding pocket compositions as well as major somatostatin binding modes. Our simulations revealed a unique behavior for the complex with SSTR5 in which somatostatin assumes a rotated conformation within the binding pocket, as compared to the other isoforms. This leads to the complete closure of the ECL2 and the establishment of distinct ligand-protein interactions, as further revealed by fingerprint analysis. Although further experimental validation is needed, overall, our findings offer detailed structural insights for the rational design of somatostatin-based drugs, particularly targeting SSTR5.

2. Results and discussion

To set-up the structures of all isoforms for our investigation, we took the experimental structures of SSTR2 and SSTR4 and AlphaFold2 models of SSTR1, SSTR3, and SSTR4 (see Methods for details). All SSTRs exhibit the typical class A GPCR structure, comprising seven transmembrane helices (TMs) alternated by three intracellular loops (ICLs) and three extracellular loops (ECLs) (Fig. S2). The primary sequence length varies from 364 residues in SSTR5 to 418 residues in SSTR3 [10] (Fig. S3). By superposing the five conformations we could discern how these differences in primary sequence translate into structural variations among isoforms. Notably: (1) SSTR2 has the shortest TM5 (36 residues compared to 41 in others); (2) SSTR4's TM6 is five residues shorter than in SSTR1, SSTR3, and SSTR5, and four residues shorter than in SSTR2; (3) TM7 is shorter in the SRIF2 family (25 residues in both SSTR1 and SSTR4) compared to the SRIF1 family (27 residues in SSTR2 and 28 residues in SSTR3, SSTR5) [30].

For clarity, receptor and ligand residues are denoted using three-letters and one-letter notations, respectively. The Ballesteros-Weinstein numbering scheme for class A GPCRs [41] is adopted throughout the paper.

To generate complexes of AlphaFold2 models of SSTR1, SSTR3, and SSTR5 with SST14, we employed a molecular docking protocol validated with available structural data (see Methods for details). In all cases, the best docking poses (Fig. S4A-E) exhibited a binding mode almost superimposed to the experimental structures of SSTR2 [32] and SSTR4 [30]. Subsequently, we conducted multi-copy all-atoms MD simulations of the five complexes, totaling 10 μs each. Hereafter, we discuss separately the stability of the systems during MD simulations and the detailed SST14/SSTR interactions.

2.1. All systems are stable during molecular dynamics simulations

As depicted in Fig. S5A-E, all complexes exhibit considerable stability throughout the MD simulations, with average root-mean-square deviation (RMSD) values of the backbone Cα below 2.5 Å. Similarly, the root-mean-square-fluctuation (RMSF) of the backbone Cα (Fig. S6A-E) indicates higher flexibility in the intra- and extracellular loops compared to the transmembrane helices, which remain highly stable. Interestingly, although the extracellular loop 2 (ECL2) is the longest one in each isoform (SSTR1, 4: 20 residues, SSTR2: 22 residues, SSTR3: 17 residues, SSTR5: 16 residues), it is not always the most flexible portion of the receptor. In SSTR3 and SSTR5, both the intracellular loop 2 (ICL2) and ECL2 exhibit fluctuations of about 2.0–2.5 Å. However, the RMSF of ECL2 is approximately 4.5 Å, while the corresponding value of ICL2 remains around 2–2.5 Å. Fluctuations involving ICL3 may be attributed to the absence of the G-protein, which was not simulated to reduce computational costs [31]. Fluctuations of the ligand heavy atoms (Fig. S7A-E) indicate its stability within the binding pocket in all cases, following the order SSTR2 = SSTR3 (3.1 ± 0.6 Å) < SSTR4 (3.5 ± 0.7 Å) < SSTR1 (4.0 ± 1.0 Å) < SSTR5 (4.8 ± 1.0 Å). Despite minor deviations, the RMSD of all replicas always reaches a plateau, demonstrating overall ligand stability. Notably, SST14 fluctuations primarily occur at the terminal portions, while residues W8 and K9 remain stably bound in the deepest part of the pocket (Fig. S8A-E) [30,32,39].

For subsequent analyses, the five MD replicas of each complex were concatenated. To further assess system stability, we monitored two geometric variables along the MD trajectories that discriminate between active and inactive forms of class A GPCRs [42,39]. These variables describe the outward displacement of TM5 and TM6 (distance δ between Cα atoms of residues in positions 5.55 and 7.46), the inward movement of TM7 at the intracellular side, and the inward shift of TM5 and TM7 at the extracellular side (angle θ between Cα atoms of positions 6.34, 6.47, and 2.41) [43–46]. As depicted in Fig. 3, all systems explore the active region of the plot (agonist-bound), with distance δ and angle θ spanning approximate ranges of 16–22 Å and 48–77°, respectively. These results further validate the overall stability and reliability of the AlphaFold2 models used for SSTR1, 3, and 5 isoforms.

2.2. ECL2 closes upon somatostatin in SSTR5 but not in the other isoforms

The ECL2 is known for its significant role in facilitating the binding and recognition processes of somatostatin receptors, impacting the stability of ligand binding [32,38,39,47–49]. In previous analyses, we

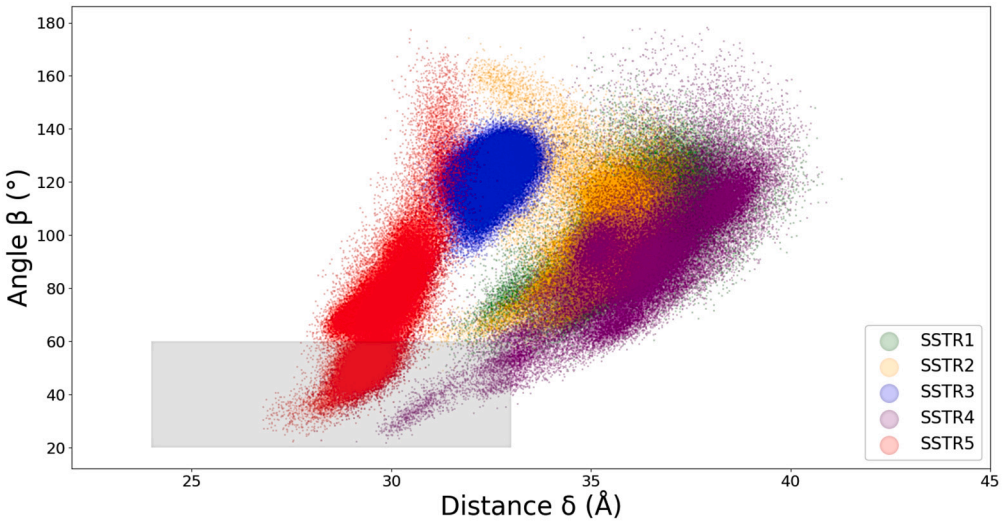

Fig. 4. Scatter plot of the ECL2 opening and closing movements. Each point of the plot refers to a frame of the MD trajectories. The results for SSTR1, 2, 3, 4, 5 are colored in green, yellow, blue, purple and red respectively. The gray box includes the frames in which the ECL2 is in the closed conformation. The distance values range from 27 to 41 Å, the angle values from 22 to 178° [39].

identified two geometric descriptors characterizing ECL2 movements: (1) the distance δ from the center of mass (COM) of the Cα atoms at the tip of ECL2 to the COM of all TMs, and (2) the angle β formed by the Cα atoms of the residue at the top of ECL2 and the COM of residues at the base of ECL2 and ECL3 (see Methods, and Table S2 for the complete list of residues) [39]. In this study, we retained these metrics but refined angle β to account for differences in ECL2 length among isoforms (see Methods). We maintained the δ threshold for the closed conformation in the range $24 < \delta < 33$ Å and updated the one for β to $20 < \beta < 60$ degrees. These quantities were computed for the entire MD trajectory of each complex and depicted in the scatter plot shown in Fig. 4.

Consistently with previous observations for SSTR2 [39], we found that in SSTR1 and SSTR3 the loop predominantly remained in the open configuration for nearly 100% and ~90% of the simulation time, respectively, likely due to steric hindrance imposed by SST14. Interestingly, in SSTR5 the loop closed approximately 29% of the total simulation time. This discrepancy, partially attributable to varying loop lengths, suggested a possible role of specific interactions between somatostatin and each isoform. Further investigation into detailed ligand-receptor interactions was thus conducted using complementary computational techniques.

2.3. Characterization of somatostatin main binding modes

To elucidate the dominant binding modes of somatostatin in different isoforms, the full MD trajectories of each complex underwent cluster analysis (see Methods). This analysis identified three significantly populated conformational clusters of SST14 for each system. Across all cases, a dominant cluster emerged (populations of 86%, 72%, 63%, 55%, and 49% for SSTR1–5, respectively) that did not substantially differ from the others, exhibiting RMSDs ranging from 0.7 Å to 3.6 Å (Table S3), reaffirming once more the overall ligand's stability. Notably, the most populated clusters of SSTR2 and SSTR4 closely resembled their respective experimental structures, with RMSD values of 0.6 Å and 1.1 Å, respectively. The structural comparison between representatives of the most populated clusters is depicted in Fig. 5, while comparisons for the second and third clusters are provided in Fig. S10A-E.

Interestingly, the major binding modes exhibited striking similarity across all isoforms, with the only exception of SSTR5. In this case, the ligand showed an average rotation of its middle and upper segments by approximately 90°. Furthermore, residue W8 appeared rotated by ~180° compared to other isoforms (Fig. S11). Consequently, the orientation of the SST14 disulfide bridge was different (Fig. 5), positioning

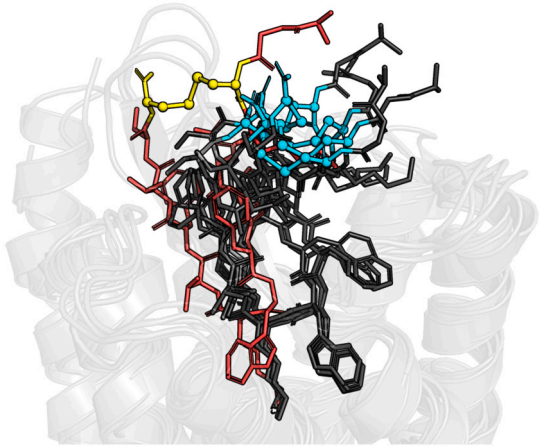

Fig. 5. Representatives of the most populated cluster of SST14 in complex with SSTR1 (84.6%), SSTR2 (71.7%), SSTR3 (63.3%), SSTR4 (55.1%), and SSTR5 (49.4%) all represented in dark gray sticks. The peculiar pose for SSTR5 is highlighted in red sticks. The yellow and cyan ball-and-sticks represent the disulfide bridge for SSTR5 and all the other isoforms, respectively.

the ligand towards TM1 and TM7 rather than TM5-6-7, as observed for SSTR1–4 (Fig. S12). This rotation of SST14 created enough room for ECL2 insertion, partially explaining its closure exclusively in the complex with SSTR5.

2.4. Detailed interactions with somatostatin

We conducted a detailed analysis of protein-ligand interactions characterizing each complex by performing an interaction fingerprint analysis on the entire MD trajectories (see Methods). Consistent with previous findings for SSTR2 [39], this analysis revealed that the central part of the ligand (residues F6 to T10) was predominantly involved in interactions with all SSTRs. This observation was expected as this portion of somatostatin deeply penetrates the binding pocket (see Fig. 4 and Fig. 5). Detailed heat maps illustrating protein residues ordered by their spatial distribution along the binding pocket and their corresponding persistence of interaction (P_{int}) are depicted in Fig. 6. The complete list of residues is provided in Table S4.

In the top region of the binding pocket, we generally observed low P_{int} values, likely due to higher solvent exposure in this region

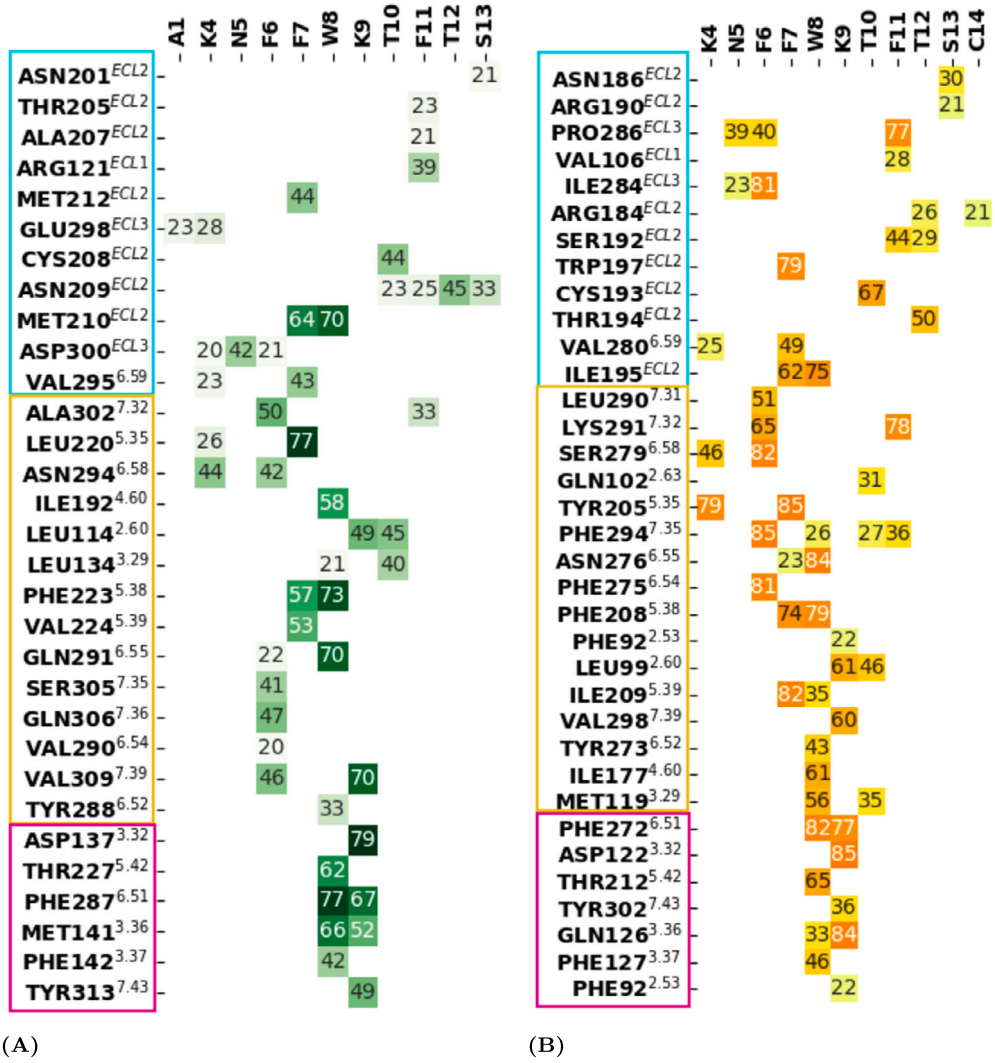

Fig. 6. Heat maps of the fingerprints analysis of **(A)** SSTR1 in green, **(B)** SSTR2 in orange, **(C)** SSTR3 in blue, **(D)** SSTR4 in purple and **(E)** SSTR5 in red. The values refer to the persistence of the interaction (in percentage) between the residues of SST14 (columns) and those of the receptors (rows). The cyan, mustard and light pink boxes include the top, middle and bottom regions respectively. Computed with ProLiF python library [50].

[39]. However, several residues exhibited notable interaction persistence (values of $P_{int} \geq 70\%$, Table S5), particularly in SSTR2, SSTR3, and SSTR4. For instance, Pro286^{ECL3} of SSTR2 played a crucial role in SST14 interaction, whereas residues in the same position of other isoforms exhibited comparatively weaker interactions.

The middle region of the binding pocket is known to host a quadruplet of residues, spanning from position 7.35 to 7.38, that is believed to be crucial for ligand recognition and selectivity (SSTR1: Ser-Gln-Leu-Ser, SSTR2: Phe-Asp-Phe-Val, SSTR3: Tyr-Phe-Leu-Val, SSTR4: Asn-His-Val-Ser, SSTR5: Tyr-Phe-Phe-Val) [51]. An important interaction stabilizing SST14 is the one involving residue F6 and residue 7.35 of the receptor [43,52]. This defines a hydrophobic sub-pocket hosting F6 [43], which is present only in the SRIF1 family due to the different nature of residue 7.35 (Phe294, Tyr295, Tyr286 for SSTR2, 3, 5 and Ser305, Asn293 for SSTR1, 4). Notably, residue F6 interaction, particularly important for ligand stabilization, exhibited high P_{int} values across all isoforms (ranging from 41% to 88%). Interestingly, in SSTR3 the interaction with F6 is further stabilized by another aromatic residue at position 7.32 (residue Phe292, $P_{int} = 81\%$) suggesting a possible knob for tuning the selectivity. Furthermore, interactions involving F7 of somatostatin and adjacent residues differed between isoforms, underscoring their potential role in isoform selectivity [31]. The same residue F7, together with W8, makes a hydrophobic interaction with residue Phe$^{5.38}$ (~ 50–70% for F7 and ~ 70–80% for W8) in all cases, with the only notable exception of SSTR5. Interestingly, residues such as Asn276$^{6.55}_{SSTR2}$ (Asn277$^{6.55}_{SSTR3}$), or Gln291$^{6.55}_{SSTR1}$ (Gln279$^{6.55}_{SSTR4}$) that appear generally crucial for receptor-ligand binding, seem to be marginal for SSTR5. Additionally, we observe a persistent hydrophobic interaction between Phe287$^{6.26}$ of SSTR5 and F11 ($P_{int} = 73\%$) that can also be found only in SSTR3 (Phe296$^{6.26}$, 79%). Moreover, according to Table S5, we found multiple unique interactions in the middle region: Phe275$^{6.54}$ in SSTR2, Try274$^{6.52}$ in SSTR3, and Phe287$^{7.36}$, Val115$^{3.28}$, Met116$^{3.29}$ in SSTR5.

In the bottom region of the pocket, interactions involving Asp$^{3.32}$ and Gln/Met$^{3.36}$ (SRIF1/SRIF2) with W8 and K9 were consistent with previous experimental observations [38,32,30,53–56,52]. The fingerprint analysis in the bottom region for SSTR5 confirms once more its peculiar behavior among all isoforms. In this case, the pattern of interactions involving the key residues W8 and K9 changes considerably, with a predominant role played by Asp$^{3.32}$ (P_{int} 78% and 85% with W8 and K9, respectively) and a minor role of Gln$^{3.36}$ that slightly interacts only with K9 (30%). Moreover, the hydrophobic interaction between W8 and Thr$^{5.42}$ (P_{int} in the range ~60%/70%) is totally missing in SSTR5. Instead, Phe$^{6.51}$ interacting with both W8 and K9 in SSTR1, 2, 3, 4 (at least 37%), in SSTR5 interacts only with K9 (~50%). Overall, these data suggest that, while in SSTR1, 2, 3, 4 residues W8 and K9

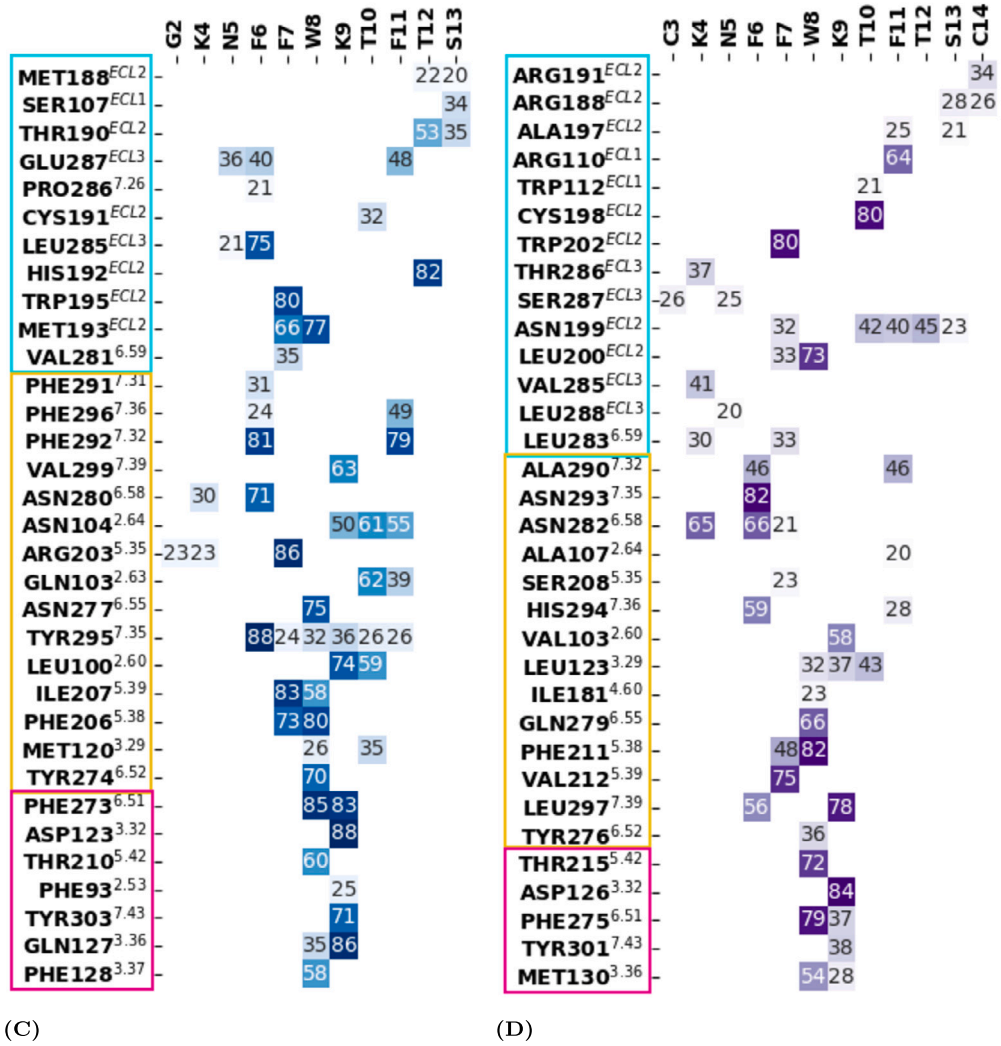

Fig. 6. (*continued*)

participate equally in the stabilization of SST14, in the case of SSTR5 the major role in keeping the ligand anchored to the bottom part of the pocket is played by K9. Notably, the fingerprint analysis revealed unique interactions characterizing each isoform in this region, suggesting isoform-specific mechanisms for ligand binding and stabilization (*i.e.*, residue Tyr303$^{7.43}$ for SSTR3 and Thr215$^{5.42}$ for SSTR4).

Taken together, the analyses presented in this study can be exploited for discovery and development of isoform-specific ligands. By carefully analyzing our results we can speculate that: (1) The SSTR5-SST14 complex displayed distinct dynamics (*e.g.*, ECL2) and protein-ligand interactions, as compared to the other isoforms. As a result, (2) maximizing interactions at TM1–TM7, instead of TM5–TM6, may enhance selectivity for SSTR5. (3) For SSTR1 we could not find any particular key of selectivity, which however is consistent with the lack of any specific ligands for this target. (4) For SSTR2 the selectivity can be improved by facilitating the interactions with ECL3 (Pro286) and Phe275$^{6.54}$ at TM6. Since this region is characterized by the presence of a hydrophobic sub-pocket, the inclusion of an aromatic ring (such as F6 of SST14) can further increase the binding affinity. (5) In SSTR3 we found two Tyr residues (Tyr274$^{6.52}$, Tyr303$^{7.43}$) specifically interacting with the bottom part of SST14. Therefore, the introduction of aromatic moieties with hydrogen bond acceptor groups in the bottom part of putative ligands can improve the selectivity towards this isoform. One example is represented by the only SSTR3 selective ligand ITF2984 that presents aromatic rings before and after the lysine residue, suggesting their localization at the bottom region of the pocket. (6) In SSTR4, Thr215$^{5.42}$ seems unique and important for the interaction with W8 of SST14. As a result, the modification of W8 with the inclusion of a hydrogen bond acceptor group (*e.g.*, 5- or 6-azaindole) can improve the specificity towards this isoform.

3. Conclusions

Somatostatin receptors represent crucial targets for precision medicine. Despite the significance of all five isoforms, specific drugs currently exist only for SSTR2. In this study, we used both experimental structures (SSTR2, 4) and AlphaFold2 models (SSTR1, 3, 5) to conduct a comprehensive computational investigation of SSTRs in complex with the endogenous ligand somatostatin. We thoroughly characterized the structure of each receptor and explored the dynamic behavior of all complexes. Notably, we observed a distinctive binding mode of somatostatin in SSTR5 compared to other isoforms. This unique configuration is primarily characterized by the rotation of somatostatin W8 residues, which also leads to the closure of the extracellular loop 2. Additionally, our fingerprint analysis of protein-ligand interactions revealed a distinct interaction pattern in SSTR5, while retaining key pharmacophore features in the bottom part of the binding pocket. Although further experimental studies are needed to validate our findings, we propose guidelines that can be exploited in the discovery and development of novel somatostatin-based pharmaceuticals for precision medicine.

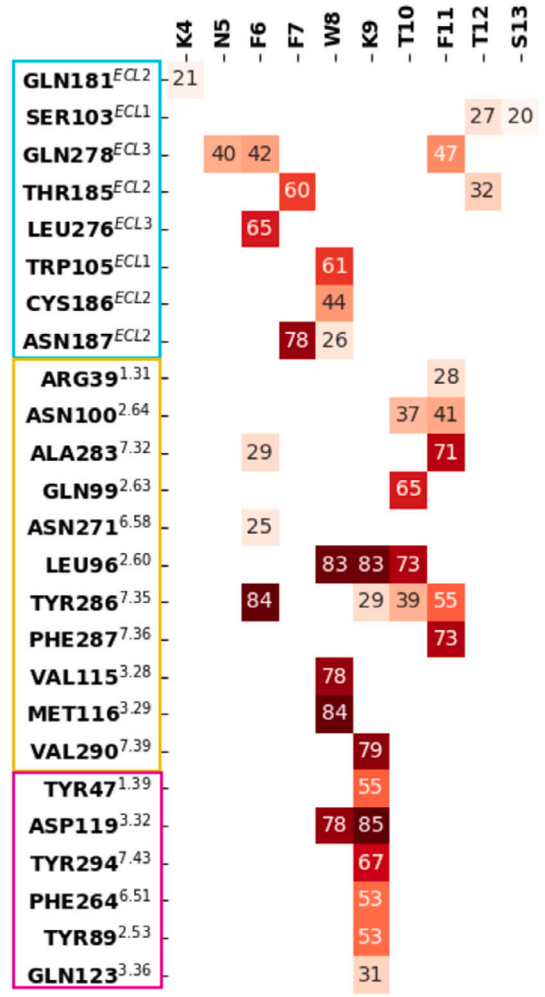

(E)

Fig. 6. (*continued*)

4. Methods

4.1. Preparation of the protein structures

The starting 3D structures of SSTR2 and SSTR4 were retrieved from the PDB [57] IDs 7T10 [32] and 7XMS [30]. Missing atoms were included via structure refinement with Modeller10.2 [58]. Missing sidechains of somatostatin from 7XMS were completed using the Vega suite [59]. The AlphaFold2 [60] models of the SSTR1, SSTR3 and SSTR5 in the active conformation were retrieved from GPCRdb [61] and first validated through ERRAT (Fig. S13) [62] and Ramachandran analyses (Fig. S14). ERRAT plots were computed with the SAVES web server and showed an overall quality factor of at least 96.8%. Ramachandran plots, generated with MolProbity [63], revealed percentages of residues starting from 97.5% in the favored region and from 99.7% in the allowed one. Models validation was further performed through the analysis of MD simulations (see Results and discussion). Structural characterization and figure preparation were done with Pymol [17].

4.2. Molecular docking and MD simulations

For the docking of somatostatin to SSTR1, 3, 5 (Fig. S4C-E), we used the HADDOCK2.4 software [64] adopting the protocol for complexes involving cyclic peptides [65]. To validate the adopted protocol we first re-docked the experimental structures of SSTR2 and SSTR4 (Fig. S4A-B) obtaining average RMSD from the experimental complexes of 1.70 Å in both cases. For the docking with SSTR3 and SSTR5, we used the bound conformation of somatostatin extracted from the experimental structure of SSTR2 (PDB ID 7T10) belonging to the subfamily SRIF1. For the docking with SSTR1, we employed a conformation of SST14 bound to SSTR4, belonging to the same subfamily SRIF2. We started from the co-structure of SSTR4 with PDB ID 7XMS, manually added the two missing N-terminal residues A1 and G2, and then minimized and optimized the reconstructed bond. We then extracted the ligand from the last step of the minimization and used this conformation for the docking with SSTR1 to mitigate potential issues or occurrence of artificial poses during the docking process. In all cases, the ligand was considered fully flexible during docking, thus encompassing all 25 rotatable bonds detected by the docking program.

In MD simulations, to reduce computational cost, we did not include the G-protein in the structures. The allosteric effect of the G-protein is supposed to have an role on major conformational rearrangements, so it is safe to assume that the lack of the G-protein in our plain μs-long MD simulations did not have an impact on the system structural features under investigation. The ionization state of the residue sidechains and the tautomeric states of histidine residues were checked by the PDB2PQR web tool [66]. The CHARMM-GUI server [67] was used to embed the complexes into a double layer of phosphatidylcholine (POPC, 70%) and cholesterol (30%) [68]. The systems were inserted in an OPC water box [69] and neutralized by adding K^+ and Cl^- ions, reaching a 0.15 M concentration. The ff19SB force field [70] was assigned to the receptors and SST14 and the lipid21 force field [71] to the POPC and cholesterol. The MD simulations were performed using Amber18 software [72].

Each system underwent an energy minimization using a combination of the steepest-descent and conjugated gradient algorithms, each comprising 2500 steps. During the minimization, positional restraints were applied to the protein-ligand complexes at a force constant of 10.0 kcalmol^{-1} Å^{-2} and to the cholesterol and phosphate groups of phosphatidylcholine molecules at a force constant of 2.5 kcalmol^{-1} Å^{-2}. NVT and NPT equilibrations followed the minimization, in which the positional restraints were incrementally reduced. The NVT equilibration consisted of two steps, with the first one lasting 125 ps and maintaining the same positional restraints used in the minimization. The second step, also lasting 125 ps, involved reducing the restraint strength to 5.0 kcalmol^{-1} Å^{-2} for the protein and ligands, while keeping it at 2.5 kcalmol^{-1} Å^{-2} for cholesterol and the phosphate groups of phosphatidylcholine molecules. The total NVT equilibration time was 250 ps. The following NPT equilibration was carried out in four steps: (1) 125 ps long using positional restraints of 2.5 kcalmol^{-1} Å^{-2} for the protein-ligand, and 1.0 kcalmol^{-1} Å^{-2} for the membrane components; (2) 500 ps long, with positional restraints of 1.0 kcalmol^{-1} Å^{-2} for the protein-ligand, and 0.5 kcalmol^{-1} Å^{-2} for the membrane components; (3) 500 ps long, but with positional restraints reduced to 0.5 kcalmol^{-1} Å^{-2} for the protein-ligand and to 0.1 kcalmol^{-1} Å^{-2} for the membrane; (4) the last one lasted 500 ps using 0.1 kcalmol^{-1} Å^{-2} for the protein-ligand and leaving the membrane unrestricted. The Langevin thermostat was utilized with a collision frequency of 1 ps^{-1} and a temperature of 310 K. The Berendsen barostat was used to maintain the pressure at 1 atm. A cut-off of 9 Å was applied, and the time step was incremented from 1 to 2 fs using the SHAKE algorithm [73]. The Particle Mesh Ewald method was employed for handling long-range electrostatic interactions [74]. The production runs were conducted for 2 μs, using the NPT ensemble and a time step of 4 fs, adopting the hydrogen mass repartition scheme [75]. To increase the sampling, five replicas were generated for each system, resulting in a total simulation time of 10 μs. The MD simulations were performed using the PMEMD module of Amber18 [72], and the trajectory frames were written every 100 ps.

MD replicas were concatenated and the CPPTRAJ software [76] was employed to perform a cluster analysis using a hierarchical algorithm [77] to group all frames into conformational clusters, according to the RMSD of somatostatin heavy atoms. In all cases, we found out that three

clusters sample significantly the different conformations adopted by the ligand (see Table S3). The ligands' RMSD values were calculated on heavy atoms, after aligning the receptors' backbone in the MD trajectories with respect to the first frame of the production run. To compute the interaction fingerprints, the ProLIF Python library [50] was employed on all frames of the MD trajectories. The numbers of interactions were combined for all replicas and converted into persistence of interactions (%). For the description of the ECL2's movements, we redefined the parameter β considering the COM of the residues at the beginning of the most flexible part of the loop instead of the ones at the base of it as done in our previous work [39]. These residues were selected by superimposing the structures retrieved by the conformational clusters (see Fig. S15A-C for better clarity).

CRediT authorship contribution statement

S.G. and G.M. designed the project. C.G. and S.G. performed the simulations and analyzed the results. C.G., S.G. and G.M. wrote the original version of the manuscript. All authors contributed and approved the final version of the manuscript.

Declaration of competing interest

The authors declare that they have no known competing financial interests or personal relationships that could have appeared to influence the work reported in this paper.

Acknowledgements

This study was partially funded by "Progetti biennali d'Ateneo Finanziati dalla Fondazione di Sardegna, annualità 2020", and the Italian Ministry of University and Research, PNRR, mission 4, component 2, investment 1.3, (Partenariati estesi alle università, ai centri di ricerca, alle aziende per il finanziamento di progetti di ricerca di base), title HEAL ITALIA, project number PE00000019, CUP: F53C22000750006.

Appendix A. Supplementary material

Supplementary material related to this article can be found online at https://doi.org/10.1016/j.csbj.2024.03.005.

References

[1] Abrahams E. Right drug-right patient-right time: personalized medicine coalition. Clin Transl Sci 2008;1(1):11–2.
[2] Collins DC, Sundar R, Lim JSJ, Yap TA. Towards precision medicine in the clinic: from biomarker discovery to novel therapeutics. Trends Pharmacol Sci 2016;38(1):25–40.
[3] Workman P, de Bono J. Targeted therapeutics for cancer treatment: major progress towards personalised molecular medicine. Curr Opin Pharmacol 2008;8(4):359–62.
[4] Moscow JA, Fojo T, Schilsky RL. The evidence framework for precision cancer medicine. Nat Rev Clin Oncol 2017;15(3):183–92.
[5] Jameson JL, Longo DL. Precision medicine–personalized, problematic, and promising. N Engl J Med 2015;372(23):2229–34.
[6] Franco Machado J, Silva RD, Melo R, Correia JDG. Less exploited GPCRs in precision medicine: targets for molecular imaging and theranostics. Molecules 2018;24(1):49.
[7] Dugger SA, Platt A, Goldstein DB. Drug development in the era of precision medicine. Nat Rev Drug Discov 2018;17(3):183–96.
[8] Jadvar H. Targeted radionuclide therapy: an evolution toward precision cancer treatment. Am J Roentgenol 2017;209(2):277–88.
[9] Duarte TT, Spencer CT. Personalized proteomics: the future of precision medicine. Proteomes 2016;4(4):29.
[10] Günther T, Tulipano G, Dournaud P, Bousquet C, Csaba Z, Kreienkamp H-J, et al. International union of basic and clinical pharmacology. CV. Somatostatin receptors: structure, function, ligands, and new nomenclature. Pharmacol Rev 2018;70(4):763–835.
[11] Gomes-Porras M, Cárdenas-Salas J, Álvarez-Escolá C. Somatostatin analogs in clinical practice: a review. Int J Mol Sci 2020;21(5):1682.
[12] McWilliam H, Li W, Uludag M, Squizzato S, Park YM, Buso N, et al. Analysis tool web services from the EMBL-EBI. Nucleic Acids Res 2013;41(Web Server issue):W597–600.
[13] Priyadarshini S, Allison DB, Chauhan A. Comprehensive assessment of somatostatin receptors in various neoplasms: a systematic review. Pharmaceutics 2022;14(7):1394.
[14] Bronstein-Sitton N. Somatostatin and the somatostatin receptors: versatile regulators of biological activity. Pathways 2006;6.
[15] Pedraza-Arévalo S, Hormaechea-Agulla D, Gómez-Gómez E, Requena MJ, Selth LA, Gahete MD, et al. Somatostatin receptor subtype 1 as a potential diagnostic marker and therapeutic target in prostate cancer. Prostate 2017;77(15):1499–511.
[16] Chen L, Hoeger C, Rivier J, Fitzpatrick VD, Vandlen RL, Tashjian Jr AH. Structural basis for the binding specificity of a sstr1-selective analog of somatostatin. Biochem Biophys Res Commun 1999;258(3):689–94.
[17] Schmid HA. Pasireotide (SOM230): development, mechanism of action and potential applications. Mol Cell Endocrinol 2008;286(1–2):69–74.
[18] Eychenne R, Bouvry C, Bourgeois M, Loyer P, Benoist E, Lepareur N. Overview of radiolabeled somatostatin analogs for cancer imaging and therapy. Molecules 2020;25(17):4012.
[19] Yu J, Cao F, Zhao X, Xie Q, Lu M, Li J, et al. Correlation and comparison of somatostatin receptor type 2 immunohistochemical scoring systems with 68Ga-DOTATATE positron emission tomography/computed tomography imaging in gastroenteropancreatic neuroendocrine neoplasms. Neuroendocrinology 2022;112(4):358–69.
[20] Modena D, Luisa MM, Sandrone G, Stevenazzi A, Vergani B, Dasgupta P, et al. Identification of a novel SSTR3 full agonist and its activity in non-functioning pituitary adenoma model. In: Endocrine abstracts, vol. 81. Bioscientifica; 2022.
[21] Corleto VD, Falconi M, Panzuto F, Milione M, De Luca O, Perri P, et al. Somatostatin receptor subtypes 2 and 5 are associated with better survival in well-differentiated endocrine carcinomas. Neuroendocrinology 2009;89(2):223–30.
[22] Somvanshi RK, Kumar U. δ-opioid receptor and somatostatin receptor-4 heterodimerization: possible implications in modulation of pain associated signaling. PLoS ONE 2014;9(1):e85193.
[23] Sándor K, Elekes K, Szabó Á, Pintér E, Engström M, Wurster S, et al. Analgesic effects of the somatostatin sst4 receptor selective agonist J-2156 in acute and chronic pain models. Eur J Pharmacol 2006;539(1–2):71–5.
[24] Terlević R, Balja MP, Tomas D, Skenderi F, Krušlin B, Vranic S, et al. Somatostatin receptor SSTR2A AND SSTR5 expression in neuroendocrine breast cancer. Ann Diagn Pathol 2019;38:62–6.
[25] Farb TB, Adeva M, Beauchamp TJ, Cabrera O, Coates DA, Meredith TD, et al. Regulation of endogenous (male) rodent GLP-1 secretion and human islet insulin secretion by antagonism of somatostatin receptor 5. Endocrinology 2017;158(11):3859–73.
[26] Li SC, Martijn C, Cui T, Essaghir A, Luque RM, Demoulin J-B, et al. The somatostatin analogue octreotide inhibits growth of small intestine neuroendocrine tumour cells. PLoS ONE 2012;7(10):e48411.
[27] Caron P, Beckers A, Cullen D, Goth M, Gutt B, Laurberg P, et al. Efficacy of the new long-acting formulation of lanreotide (lanreotide autogel) in the management of acromegaly. J Clin Endocrinol Metab 2002;87(1):99–104.
[28] Bolanowski M, Kałużny M, Witek P, Jawiarczyk-Przybyłowska A. Pasireotide—a novel somatostatin receptor ligand after 20 years of use. Rev Endocr Metab Disord 2022;23(3):601–20.
[29] Madan A, Markison S, Betz SF, Krasner A, Luo R, Jochelson T, et al. Paltusotine, a novel oral once-daily nonpeptide SST2 receptor agonist, suppresses GH and IGF-1 in healthy volunteers. Pituitary 2022:1–12.
[30] Zhao W, Han S, Qiu N, Feng W, Lu M, Zhang W, et al. Structural insights into ligand recognition and selectivity of somatostatin receptors. Cell Res 2022;32(8):761–72.
[31] Gervasoni S, Öztürk I, Guccione C, Bosin A, Ruggerone P, Malloci G. Interaction of radiopharmaceuticals with somatostatin receptor 2 revealed by molecular dynamics simulations. J Chem Inf Model 2023;63(15):4924–33.
[32] Robertson MJ, Meyerowitz JG, Panova O, Borrelli K, Skiniotis G. Plasticity in ligand recognition at somatostatin receptors. Nat Struct Mol Biol 2022;29(3):210–7.
[33] Nagarajan SK, Babu S, Madhavan T. Theoretical analysis of somatostatin receptor 5 with antagonists and agonists for the treatment of neuroendocrine tumors. Mol Divers 2017;21:367–84.
[34] Nagarajan SK, Babu S, Sohn H, Madhavan T. Molecular-level understanding of the somatostatin receptor 1 (SSTR1)–ligand binding: a structural biology study based on computational methods. ACS Omega 2020;5(33):21145–61.
[35] Nagarajan SK, Babu S, Devaraju P, Sohn H, Madhavan T. Structure and dynamics of the somatostatin receptor 3-ligand binding in the presence of lipids examined using computational structural biology methods. Proteins 2022;90(3):704–19.
[36] Dzimbova T, Wesselinova D, Naydenova E, Milanov P. Computer modelling of all types of somatostatin receptors. J Chem Technol Metall 2020;55(2):272–6.
[37] Börzsei R, Zsidó BZ, Bálint M, Helyes Z, Pintér E, Hetényi C. Exploration of somatostatin binding mechanism to somatostatin receptor subtype 4. Int J Mol Sci 2022;23(13):6878.
[38] Robertson MJ, Papasergi-Scott MM, He F, Seven AB, Meyerowitz JG, Panova O, et al. Structure determination of inactive-state GPCRs with a universal nanobody. Nat Struct Mol Biol 2022;29(12):1188–95.
[39] Gervasoni S, Guccione C, Fanti V, Bosin A, Cappellini G, Golosio B, et al. Molecular simulations of SSTR2 dynamics and interaction with ligands. Sci Rep 2023;13(1):4768.
[40] He XH, You CZ, Jiang HL, Jiang Y, Xu HE, Cheng X. AlphaFold2 versus experimental structures: evaluation on G protein-coupled receptors. Acta Pharmacol Sin 2023;44(1):1–7.

[41] Ballesteros JA, Weinstein H. Integrated methods for the construction of three-dimensional models and computational probing of structure-function relations in G protein-coupled receptors. In: Methods in neurosciences, vol. 25. Elsevier; 1995. p. 366–428.
[42] Lu S, He X, Yang Z, Chai Z, Zhou S, Wang J, et al. Activation pathway of a G protein-coupled receptor uncovers conformational intermediates as targets for allosteric drug design. Nat Commun 2021;12(1):4721.
[43] Zhou Q, Yang D, Wu M, Guo Y, Guo W, Zhong L, et al. Common activation mechanism of class a GPCRs. eLife 2019;8:e50279.
[44] Hauser AS, Kooistra AJ, Munk C, Heydenreich FM, Veprintsev DB, Bouvier M, et al. GPCR activation mechanisms across classes and macro/microscales. Nat Struct Mol Biol 2021;28(11):879–88.
[45] Weis WI, Kobilka BK. The molecular basis of G protein–coupled receptor activation. Annu Rev Biochem 2018;87:897–919.
[46] Latorraca NR, Venkatakrishnan A, Dror RO. GPCR dynamics: structures in motion. Chem Rev 2017;117(1):139–55.
[47] Wheatley M, Wootten D, Conner MT, Simms J, Kendrick R, Logan RT, et al. Lifting the lid on GPCRs: the role of extracellular loops. Br J Pharmacol 2012;165(6):1688–703.
[48] Nicoli A, Dunkel A, Giorgino T, de Graaf C, Di Pizio A. Classification model for the second extracellular loop of class a GPCRs. J Chem Inf Model 2022;62(3):511–22.
[49] Woolley MJ, Conner AC. Understanding the common themes and diverse roles of the second extracellular loop (ECL2) of the GPCR super-family. Mol Cell Endocrinol 2017;449:3–11.
[50] Bouysset C, Fiorucci S. ProLIF: a library to encode molecular interactions as fingerprints. J Cheminform 2021;13:1–9.
[51] Møller LN, Stidsen CE, Hartmann B, Holst JJ. Somatostatin receptors. Biochim Biophys Acta, Biomembr 2003;1616(1):1–84.
[52] Zhao J, Fu H, Yu J, Hong W, Tian X, Qi J, et al. Prospect of acromegaly therapy: molecular mechanism of clinical drugs octreotide and paltusotine. Nat Commun 2023;14(1):962.
[53] Chen LN, Wang WW, Dong YJ, Shen DD, Guo J, Yu X, et al. Structures of the endogenous peptide- and selective non-peptide agonist-bound SSTR2 signaling complexes. Cell Res 2022;32(8):785–8.
[54] Heo Y, Yoon E, Jeon YE, Yun JH, Ishimoto N, Woo H, et al. Cryo-EM structure of the human somatostatin receptor 2 complex with its agonist somatostatin delineates the ligand-binding specificity. eLife 2022;11:e76823.
[55] Bo Q, Yang F, Li Y, Meng X, Zhang H, Zhou Y, et al. Structural insights into the activation of somatostatin receptor 2 by cyclic SST analogues. Cell Discov 2022;8(1):47.
[56] Chen S, Teng X, Zheng S. Molecular basis for the selective G protein signaling of somatostatin receptors. Nat Chem Biol 2023;19(2):133–40.
[57] Berman HM, Westbrook J, Feng Z, Gilliland G, Bhat TN, Weissig H, et al. The protein data bank. Nucleic Acids Res 2000;28(1):235–42.
[58] Eramian M-yS, Pieper U, Sali A. Comparative protein structure modeling using modeller. Curr Protoc Bioinform 2006;5(1–5):6.
[59] Pedretti A, Mazzolari A, Gervasoni S, Fumagalli L, Vistoli G. The VEGA suite of programs: an versatile platform for cheminformatics and drug design projects. Bioinformatics 2021;37(8):1174–5.
[60] Jumper J, Evans R, Pritzel A, Green T, Figurnov M, Ronneberger O, et al. Highly accurate protein structure prediction with AlphaFold. Nature 2021;596(7873):583–9.
[61] Pándy-Szekeres G, Caroli J, Mamyrbekov A, Kermani AA, Keserű GM, Kooistra AJ, et al. GPCRdb in 2023: state-specific structure models using AlphaFold2 and new ligand resources. Nucleic Acids Res 2023;51(D1):D395–402.
[62] Colovos C, Yeates TO. Verification of protein structures: patterns of nonbonded atomic interactions. Protein Sci 1993;2(9):1511–9.
[63] Williams CJ, Headd JJ, Moriarty NW, Prisant MG, Videau LL, Deis LN, et al. MolProbity: more and better reference data for improved all-atom structure validation. Protein Sci 2018;27(1):293–315.
[64] Van Zundert G, Rodrigues J, Trellet M, Schmitz C, Kastritis P, Karaca E, et al. The HADDOCK2.2 web server: user-friendly integrative modeling of biomolecular complexes. J Mol Biol 2016;428(4):720–5.
[65] Charitou V, Van Keulen SC, Bonvin AM. Cyclization and docking protocol for cyclic peptide–protein modeling using HADDOCK2.4. J Chem Theory Comput 2022;18(6):4027–40.
[66] Jurrus E, Engel D, Star K, Monson K, Brandi J, Felberg LE, et al. Improvements to the APBS biomolecular solvation software suite. Protein Sci 2018;27(1):112–28.
[67] Jo S, Kim T, Iyer VG, Im W. CHARMM-GUI: a web-based graphical user interface for CHARMM. J Comput Chem 2008;29(11):1859–65.
[68] Saeedimasine M, Montanino A, Kleiven S, Villa A. Role of lipid composition on the structural and mechanical features of axonal membranes: a molecular simulation study. Sci Rep 2019;9(1):8000.
[69] Izadi S, Anandakrishnan R, Onufriev AV. Building water models: a different approach. J Phys Chem Lett 2014;5(21):3863–71.
[70] Tian C, Kasavajhala K, Belfon KA, Raguette L, Huang H, Migues AN, et al. ff19SB: amino-acid-specific protein backbone parameters trained against quantum mechanics energy surfaces in solution. J Chem Theory Comput 2019;16(1):528–52.
[71] Dickson CJ, Walker RC, Gould IR. Lipid21: complex lipid membrane simulations with AMBER. J Chem Theory Comput 2022;18(3):1726–36.
[72] Salomon-Ferrer R, Case DA, Walker RC. An overview of the AMBER biomolecular simulation package. Wiley Interdiscip Rev Comput Mol Sci 2013;3(2):198–210.
[73] Kräutler V, Van Gunsteren WF, Hünenberger PH. A fast shake algorithm to solve distance constraint equations for small molecules in molecular dynamics simulations. J Comput Chem 2001;22(5):501–8.
[74] Darden T, York D, Pedersen L. Particle mesh Ewald: an $n \cdot \log(n)$ method for Ewald sums in large systems. J Chem Phys 1993;98(12):10089–92.
[75] Jung J, Kasahara K, Kobayashi C, Oshima H, Mori T, Sugita Y. Optimized hydrogen mass repartitioning scheme combined with accurate temperature/pressure evaluations for thermodynamic and kinetic properties of biological systems. J Chem Theory Comput 2021;17(8):5312–21.
[76] Roe DR, Cheatham III TE. PTRAJ and CPPTRAJ: software for processing and analysis of molecular dynamics trajectory data. J Chem Theory Comput 2013;9(7):3084–95.
[77] Shao J, Tanner SW, Thompson N, Cheatham TE. Clustering molecular dynamics trajectories: 1. Characterizing the performance of different clustering algorithms. J Chem Theory Comput 2007;3(6):2312–34.